DOI: 10.1002/ejic.201000821

New Chlorido(dimethyl sulfoxide)iridium(III) Complexes with N^6-Substituted Adenines – Kinetic N(7) versus Thermodynamic N(9) Coordinated Adenine Isomers

Angel García-Raso,*[a] Juan J. Fiol,[a] Francisca M. Albertí,[a] Yolanda Lagos,[a] Marta Torres,[a] Miquel Barceló-Oliver,[a] María J. Prieto,[b] Virtudes Moreno,[b] Ignasi Mata,[c] Elies Molins,[c] Carolina Estarellas,[a] Antonio Frontera,*[a] David Quiñonero,[a] and Pere M. Deyà[a]

Keywords: Iridium / Coordination modes / Amino acids / Structure elucidation / Density functional calculations

New chlorido(dimethyl sulfoxide)iridium(III) complexes with N^6-substituted adenine derivatives: $[Ir^{III}Cl_4(DMSO\text{-}\kappa S)\{H\text{-}AdeC_x\text{–}\kappa N(7)\}]\cdot nH_2O$ [x = 3, *n* = 3 for **1**; x = 4, *n* = 0.5 and 3 for **2a** and **2b**, respectively; x = 5, *n* = 0 for **3**; *x* = 10, *n* = 0.33 for **4**] and $[Ir^{III}Cl_4(DMSO\text{-}\kappa S)\{H\text{-}AdeC_x\text{–}\kappa N(9)\}]$ [x = 3 for **5**; x = 4 for **6**, x = 5 for **7**; x = 10 for **8**] have been synthesized and characterized by spectroscopic techniques and by single-crystal X-ray diffraction studies (**1**, **2b** and **5**). In all cases, iridium shows octahedral geometry and is coordinated to four chlorido ligands and one S atom from dimethyl sulfoxide (DMSO-κS). The coordination sphere of the metal is completed by the N^6-substituted adenine molecule. Two different coordination modes are observed: (i) the ligand is protonated at N(1) and coordinated through N(7) (complexes **1**–**4**); (ii) the adenine is protonated at N(3) and coordinated through N(9) (complexes **5**–**8**). The kinetic/thermodynamic mechanisms that yield the different coordination products have been studied by using DFT calculations. Electrophoretic mobility studies and atomic force microscopy (AFM) investigation of the interaction between complexes **1**, **5**, **8** and plasmid pBR322 DNA have been performed.

Introduction

Organoiridium chemistry is in great development in organic synthesis and catalysis,[1] and iridium(III) cyclometalated compounds have been extensively applied in the design and preparation of light-emitting diodes,[2,3] photoactivated agents in redox reactions with DNA[4] or luminescent labels and sensor molecules for biological purposes.[5,6] Furthermore, although several organometallic Ir^{III} compounds with ligands of biological interest have been described,[7–10] few studies of non-organometallic Ir^{III} complexes have been reported.[11–15]

On the other hand, Ru^{III} complexes, [LH][*trans*-$Ru^{III}Cl_4$(DMSO-κS)(L)] (L = nitrogenated ligand), such as NAMI-A [ImH][*trans*-$Ru^{III}Cl_4$(DMSO-κS)(Im)] (Im = imidazole) or KP1019 [IndH][*trans*-$Ru^{III}Cl_4(Ind)_2$] (Ind = indazole) show selective antimetastatic properties or specific antitumour action.[16–18] Moreover, several Ir^{III}- and Rh^{III}-related compounds have proved to be potent in vitro cytotoxic agents,[19,20] although similar "NAMI-A"-Ir^{III} or Rh^{III} complexes have been found to be inactive,[11,12,21] which has been related to the lack of lability for ligand substitution and redox properties of the metal centre. In this way, the more inert Ir^{III} compounds could be useful as trace systems to study the route of Ru^{III} analogues or designed complexes to deliver an active ligand to a specific receptor.

As a continuation of our work on the zwitterionic system $[MCl_4(DMSO\text{-}\kappa S)HL]$ (M = Ru^{III}, Ir^{III}; L = nitrogenated ligand),[14,22,23] we have explored the synthesis of new iridium(III) complexes with N^6-substituted adenines that present cytokinin activity.[24,25] Natural cytokinins (CK) are modified adenine molecules with a side chain at the N^6-position that are involved in most aspects of plant growth and development and exhibit interesting biological properties.[26,27] Moreover, CK–metal complexes (with Zn^{II}, Cu^{II}, Fe^{II}, Pt^{II}, among others) show significant cytotoxic activity.[28,29]

In this paper we report the synthesis and characterization by X-ray diffraction of two types of isomeric complexes with N^6-substituted adenines, N(7)–Ir and N(9)–Ir

[a] Departament de Química, Universitat de les Illes Balears and Inst. Hlth. Sci. Res. IUNICS,
Campus UIB, Ctra.Valldemossa, km 7.5, 07122 Palma de Mallorca, Spain
Fax: +34-971173426
E-mail: angel.garcia-raso@uib.es
toni.frontera@uib.es
[b] Departaments de Química Inorgànica i Microbiologia, Universitat de Barcelona,
Campus de Pedralbes, 08028 Barcelona, Spain
[c] Institut de Ciència de Materials de Barcelona (CSIC), Campus UAB, 08193 Bellaterra, Spain

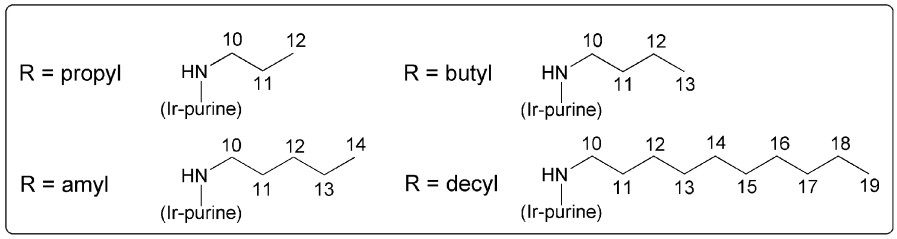

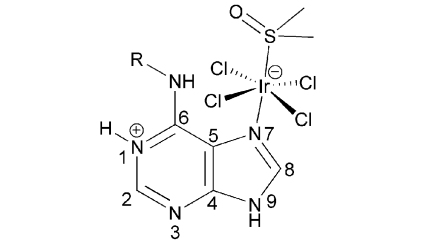

$[Ir^{III}Cl_4(DMSO)\text{-}\kappa S)[H\text{-}AdeC_x\text{-}\kappa N(7)]]\cdot nH_2O$

1	$x = 3$	$n = 3$
2a	$x = 4$	$n = 0.5$
2b	$x = 4$	$n = 3$
3	$x = 5$	$n = 0$
4	$x = 10$	$n = 0.33$

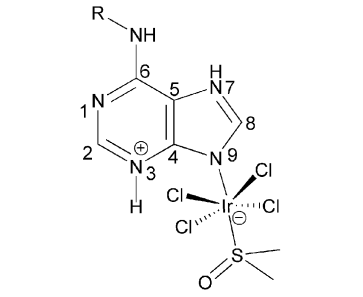

$[Ir^{III}Cl_4(DMSO)\text{-}\kappa S)[H\text{-}AdeC_x\text{-}\kappa N(9)]]$

5	$x = 3$
6	$x = 4$
7	$x = 5$
8	$x = 10$

Scheme 1. Numbering scheme of compounds **1**–**8**.

(Scheme 1), which are obtained under different experimental reaction conditions. We also report a theoretical study, which is useful to explain the different isomers obtained depending on the experimental conditions (kinetic or thermodynamic). Preliminary electrophoretic mobility and atomic force microscopy (AFM) studies of the interaction between complexes **1**, **5** and **8** and plasmid pBR322 DNA are also reported. Their antiproliferative activity was assayed against the HL-60 tumour cell line.

Results and Discussion

Synthesis

As already described,[17] in the *trans*-$[Ru^{III}Cl_4(DMSO)_2]^-$ precursor, the remarkable *trans*-influencing effect of the two DMSO molecules coordinated through the sulfur atom favours the substitution of one of them by heterocyclic nitrogenated ligands. In some cases, hydrolysis of one chlorido ligand favours the formation of *mer*-$[MCl_3(DMSO)(H_2O)\text{-}L]$, which can be possible by access of a second ligand L.

Initially, the synthesis of analogous Ir^{III} complexes was performed by the methods use for Ru^{III} complexes,[22,23] but only the outer-sphere compound, that is $[H\text{-}AdeC_3][Ir^{III}Cl_4(DMSO\text{-}\kappa S)_2]$ (**1′**), was isolated and spectroscopically characterized as expected for the more inert Ir^{III} complexes. For this reason, the temperature was increased to 40 °C (reaction time 3–4 d). In this way, zwitterionic $[Ir^{III}Cl_4(DMSO\text{-}\kappa S)\{H\text{-}AdeC_x\text{-}\kappa N(7)\}]$ complexes, coordinated through N(7) and protonated at N(1), were obtained (complexes **1**–**4**). On the other hand, by heating at 90 °C (reaction time 8 h), the N(9)–Ir isomers, protonated at N(3), were isolated (complexes **5**–**8**).

Description of X-ray Crystallographic Structures

Selected crystallographic data are shown in the Experimental Section. ORTEP representations of complexes $[Ir^{III}Cl_4(DMSO\text{-}\kappa S)\{H\text{-}AdeC_3\text{-}\kappa N(7)\}]\cdot 3H_2O$ (**1**), $[Ir^{III}Cl_4(DMSO\text{-}\kappa S)\{H\text{-}AdeC_4\text{-}\kappa N(7)\}]\cdot 3H_2O$ (**2b**) and $[Ir^{III}Cl_4(DMSO\text{-}\kappa S)\{H\text{-}AdeC_3\text{-}\kappa N(9)\}]$ (**5**) are shown in Figure 1. These three zwitterionic inner-sphere complexes present a distorted octahedral geometry around the Ir^{III} metal ion, where the basal plane is occupied by four chlorido ligands and the axial positions by a DMSO ligand coordinated through S (κS) and the corresponding N^6-substituted adenine [coordinated through N(7) in complexes **1** and **2b** and through N(9) in **5**]. All Ir^{III} complexes show metal–nitrogen [2.1172(10) for **1**, 2.096(10) for **2b** and 2.069(7) Å for **5**] and metal–sulfur [2.2459(4) for **1**, 2.244(3) for **2b** and 2.232(2) Å for **5**] bond lengths comparable to those of related com-

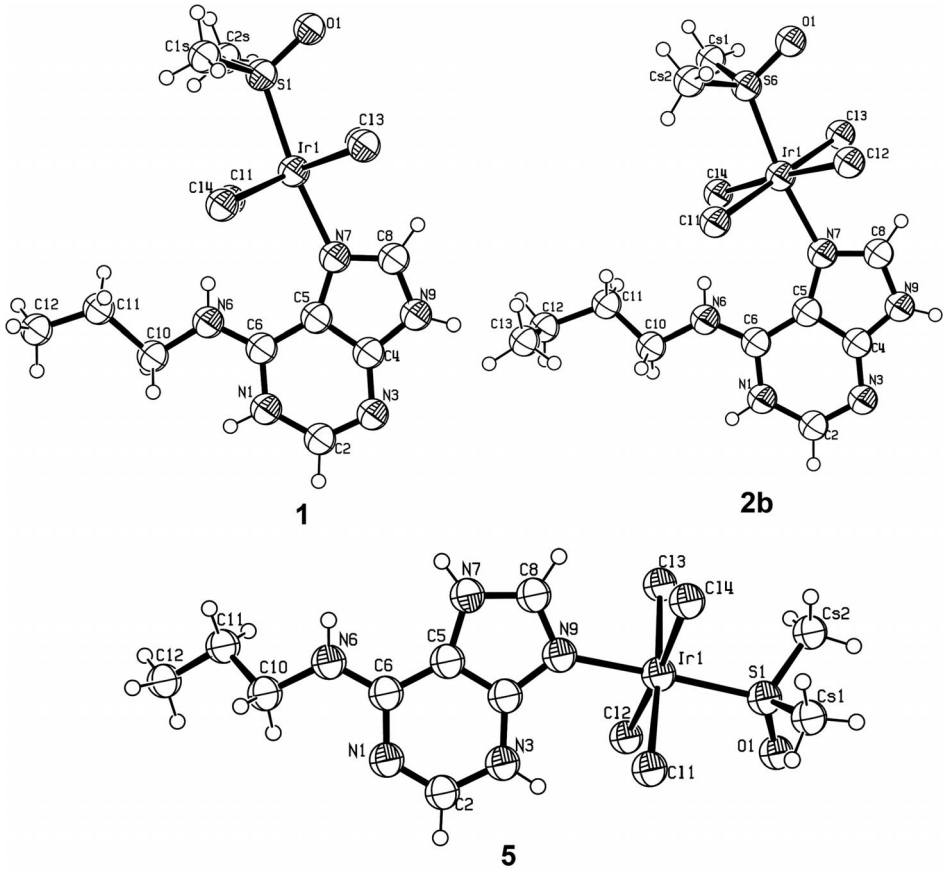

Figure 1. ORTEP drawings of complexes **1**, **2b** and **5**. Displacement ellipsoids are drawn at the 50% probability level, and H atoms are drawn as circles of arbitrary radii. Water molecules are omitted for clarity.

plexes of Ru^{III}[17,22,23] and Ir^{III}[11,12] already described. The same can be said for the Ir–Cl bond lengths [ranging from 2.3382(6) to 2.3618(7) Å for **1**, 2.340(3) to 2.356(3) Å for **2b** and 2.344(3) to 2.358(1) Å for **5**]. As can be observed, Ir–N and Ir–S distances in complex **5** [coordinated through N(9)] are slightly shorter than those in complexes **1** and **2b** [coordinated through N(7)].

Finally, the *cis* angles around the metal ion vary between 90.27(3) and 92.55(3)° for **1**, 90.00(12) and 92.55(3)° for **2** and 89.10(10) and 92.47(10)° for **5**, while the *trans* angles are between 176.969(11) and 178.07(1)° for **1**, 176.89(11) and 177.77(12)° for **2** and 175.87(9) and 176.33(6)° for **5**. Selected bond lengths and angles are shown in Table 1.

As previously described with Ru^{III} analogues,[23] the most commonly observed coordination site of N^6-substituted adenines is N(9). In our hands, the corresponding Ir^{III} derivatives, at 40 °C, yield the N(7)–Ir complex, while at higher temperatures (90 °C) N(9)–Ir complexes can be isolated. A possible reason for the initial coordination at N(7) of the ligand at gentle reaction conditions is that such binding allows relatively strong intramolecular hydrogen bonds.[30,31] Thus, in complexes **1** and **2b**, the N(1)-protonated adenine ligand is involved in intramolecular hydrogen bonding with two *cis* chlorido ligands through the exocyclic nitrogen atom N(6) [N(6)–H···Cl distances from 2.43 to 2.74 Å and angles from 112.0 to 147.8° in complex **1**; distances from 2.41 to 2.62 Å and angles from 122.3 to 152.8° in complex **2b**].

Although in N(9)-metalated/substituted adenine complexes the preferred protonation site is N(1) under acidic conditions,[32–35] several examples of N^6-substituted adenine complexes coordinated through N(9) and protonated at N(3) have been reported.[23,36,37] In our hands, N(9)–Ir complex **5** has the protonation site at N(3). It has been proposed that this protonation site is stabilized by weak intramolecular hydrogen bonds [distances N(3)–H···Cl 2.57–2.88 Å; angles N(3)–H···Cl 126.1 and 114.4°, respectively]. Furthermore, this pattern is confirmed by comparing the internal angles C2–N3–C4 and C2–N1–C6 with neutral adenine [110.8(1) and 118.8(2)°].[38,39] Larger bond angles of C2–N3–C4 [N(9)–Ir isomers] or C2–N1–C6 (N7–Ir isomers) are consistent with the protonation at N(3) or N(1), respectively (see Table 1).

The crystal packing, in complexes **1** and **2b** is dictated by intermolecular hydrogen bonds between O(DMSO) and chlorido ligands, and water molecules of crystallization are present in both structures. On the other hand, three intermolecular interactions among complex units principally determine the crystal packing of complex **5** [N(6)–H···O(1) 2.19 Å; N(7)–H···O(1) 1.95 Å; N(7)···Cl(2) 2.72 Å].

Table 1. Selected bond lengths [Å] and angles [°] for compounds **1**, **2b** and **5**.

1			
Ir(1)–N(7)	2.1172(10)	Ir(1)–S(1)	2.2459(4)
Ir(1)–Cl(1)	2.3618(7)	Ir(1)–Cl(2)	2.3574(7)
Ir(1)–Cl(3)	2.3517(7)	Ir(1)–Cl(4)	2.3382(6)
N(7)–Ir(1)–S(1)	172.84(2)	N(7)–Ir(1)–Cl(4)	90.27(3)
S(1)–Ir(1)–Cl(4)	94.03(2)	N(7)–Ir(1)–Cl(3)	86.29(3)
S(1)–Ir(1)–Cl(3)	88.08(2)	Cl(4)–Ir(1)–Cl(3)	88.87(3)
N(7)–Ir(1)–Cl(2)	88.51(3)	S(1)–Ir(1)–Cl(2)	87.32(2)
Cl(4)–Ir(1)–Cl(2)	178.07(1)	Cl(3)–Ir(1)–Cl(2)	92.55(3)
N(7)–Ir(1)–Cl(1)	90.80(3)	S(1)–Ir(1)–Cl(1)	94.89(2)
Cl(4)–Ir(1)–Cl(1)	90.29(3)	Cl(3)–Ir(1)–Cl(1)	176.969(11)
Cl(2)–Ir(1)–Cl(1)	88.22(3)	C(2)–N(1)–C(6)	123.41(9)
		C(2)–N(3)–C(4)	111.56(12)
2b			
Ir(1)–N(7)	2.096(10)	Ir(1)–S(6)	2.244(3)
Ir(1)–Cl(1)	2.340(3)	Ir(1)–Cl(2)	2.346(2)
Ir(1)–Cl(3)	2.356(3)	Ir(1)–Cl(4)	2.349(3)
N(7)–Ir(1)–S(6)	172.5(3)	N(7)–Ir(1)–Cl(4)	91.20(3)
S(6)–Ir(1)–Cl(4)	94.79(12)	N(7)–Ir(1)–Cl(3)	87.80(3)
S(6)–Ir(1)–Cl(3)	87.30(12)	Cl(4)–Ir(1)–Cl(3)	88.00(12)
N(7)–Ir(1)–Cl(2)	86.30(3)	S(6)–Ir(1)–Cl(2)	88.22(12)
Cl(4)–Ir(1)–Cl(2)	176.89(11)	Cl(3)–Ir(1)–Cl(2)	92.89(12)
N(7)–Ir(1)–Cl(1)	91.20(3)	S(6)–Ir(1)–Cl(1)	93.84(12)
Cl(4)–Ir(1)–Cl(1)	90.00(12)	Cl(3)–Ir(1)–Cl(1)	177.77(12)
Cl(2)–Ir(1)–Cl(1)	89.05(13)	C(2)–N(1)–C(6)	123.80(12)
		C(2)–N(3)–C(4)	112.6(11)
5			
Ir(1)–N(9)	2.069(7)	Ir(1)–S(1)	2.232(2)
Ir(1)–Cl(1)	2.351(7)	Ir(1)–Cl(2)	2.358(2)
Ir(1)–Cl(3)	2.358(1)	Ir(1)–Cl(4)	2.344(3)
N(9)–Ir(1)–S(1)	177.1(2)	N(9)–Ir(1)–Cl(4)	88.80(2)
S(1)–Ir(1)–Cl(4)	90.59(9)	N(9)–Ir(1)–Cl(3)	88.30(2)
S(1)–Ir(1)–Cl(3)	94.45(9)	Cl(4)–Ir(1)–Cl(3)	88.33(10)
N(9)–Ir(1)–Cl(2)	87.90(2)	S(1)–Ir(1)–Cl(2)	92.83(8)
Cl(4)–Ir(1)–Cl(2)	175.87(9)	Cl(3)–Ir(1)–Cl(2)	89.10(10)
N(9)–Ir(1)–Cl(1)	88.10(2)	S(1)–Ir(1)–Cl(1)	89.13(9)
Cl(4)–Ir(1)–Cl(1)	92.47(10)	Cl(3)–Ir(1)–Cl(1)	176.33(9)
Cl(2)–Ir(1)–Cl(1)	84.90(9)	C(2)–N(1)–C(6)	121.1(8)
		C(2)–N(3)–C(4)	117.9(8)

NMR Spectroscopic Studies: ^{1}H and ^{13}C NMR Spectra

^{1}H NMR spectra allow an easy identification of the two different isomers, N(7)–Ir or N(9)–Ir (see Scheme 2). Additional 2D NMR spectroscopic experiments (^{1}H, ^{13}C HMBC) for complexes **1**, **5** and for the corresponding N^6-alkyladenine ligand (H-AdeC$_3$) have been performed, in order to obtain an unequivocal assignment of the adenine signals (^{1}H and ^{13}C). The assignments of complexes **2**–**4** and **6**–**8** have been carried out by comparison of these data. Furthermore, it must be mentioned that the structures of complexes **1** and **5** have been solved by X-ray diffraction.

Selected ^{1}H NMR spectroscopic data for complexes **1**–**8** are shown in Table 2. All complexes (comparing with the protonated ligands) show downfield shifts corresponding to 8-H, which is in agreement with the coordination site, always in the imidazole moiety. These values were higher in N(9)–Ir complexes ($\Delta\delta$ = +0.33 to +0.37 ppm) than those in the isomeric N(7)–Ir derivatives ($\Delta\delta$ = +0.10 to +0.27 ppm). On the other hand, the behaviour of the pyrimidine moiety of the adenine ligand is completely different. Whist the N(7) complexes are characterized by an upfield shift at 2-H ($\Delta\delta$ = –0.18 to –0.30 ppm), the corresponding N(9) structures present a downfield shift corresponding to 2-H ($\Delta\delta$ = +0.14 to +0.17 ppm). The C(10)–H$_2$ proton signal is broad and generally hidden in the residual water signal; for this reason, it is generally not assigned in spectra. On the other hand, the signal corresponding to the methyl groups of dimethyl sulfoxide, present in all complexes, appears at approximately 3.30–3.40 [s, 6 H, $(CH_3)_2SO$] {^{1}H–NMR ([D$_6$]DMSO)} and at 41–42 ppm {^{13}C NMR ([D$_6$]-DMSO) [$(CH_3)_2SO$]}.[40]

A comparison of the ^{13}C NMR spectroscopic data of complexes **1** and **5** with those of the protonated ligands shows a downfield effect for C-8, which is also in accordance with the coordination of Ir^{III} through the imidazole ring.

Conversion of the N(7)–Ir Complex to the Isomeric N(9) Coordinated Product

Because of the low water solubility of all synthesized coordinated Ir^{III} complexes, it was impossible to carry out kinetic experiments by using ^{1}H NMR spectroscopy as a tool to investigate the changes in the coordination sites of adenine–Ir complexes. To observe this change, we carried out an experiment in two different NMR tubes under the same conditions (0.05 mmol of the ligand [H-AdeC$_3$]Cl and 0.05 mmol of the starting complex [$(DMSO)_2H$][*trans*-Ir^{II}Cl$_4$$(DMSO)_2$] were dissolved in 1.5 mL of D_2O). Both NMR tubes were heated at 40 °C for 36 h. After 14 h, orange crystals appeared in both tubes, and the ^{1}H NMR spectrum of the solution showed the two typical aromatic signals corresponding to the N(7) complex **1** as the main product, which disappeared as the amount of orange crystals in the tube increased. Crystals from one of the NMR tubes were filtered off, washed with cold acetone and dried under vacuum. The ^{1}H NMR spectra ([D$_6$]DMSO) of these crystals clearly showed that the compound was N(7)-coordinated Ir^{III} complex **1**.

On the other hand, the other NMR tube was heated for an additional 6 h at 90 °C, and a change from orange crystalline material to orange microcrystalline precipitate occurred slowly. The ^{1}H NMR spectrum of the solution only showed very weak signals assigned to the N(7)-coordinated Ir^{III} complex. At the end of the reaction, the orange microcrystalline precipitate, deposited at the bottom of the tube, was filtered off, washed with cold acetone and dried in vacuo. ^{1}H NMR spectra ([D$_6$]DMSO) of this solid showed the two aromatic signals corresponding to N(9)-coordinated Ir^{III} complex **5**.

Infrared and Electronic Spectra

The infrared spectra of the inner-sphere complexes **1**–**8** were compared with those of protonated N^6-substituted adenines. Tentative band assignments [cm^{-1}] for the ligands

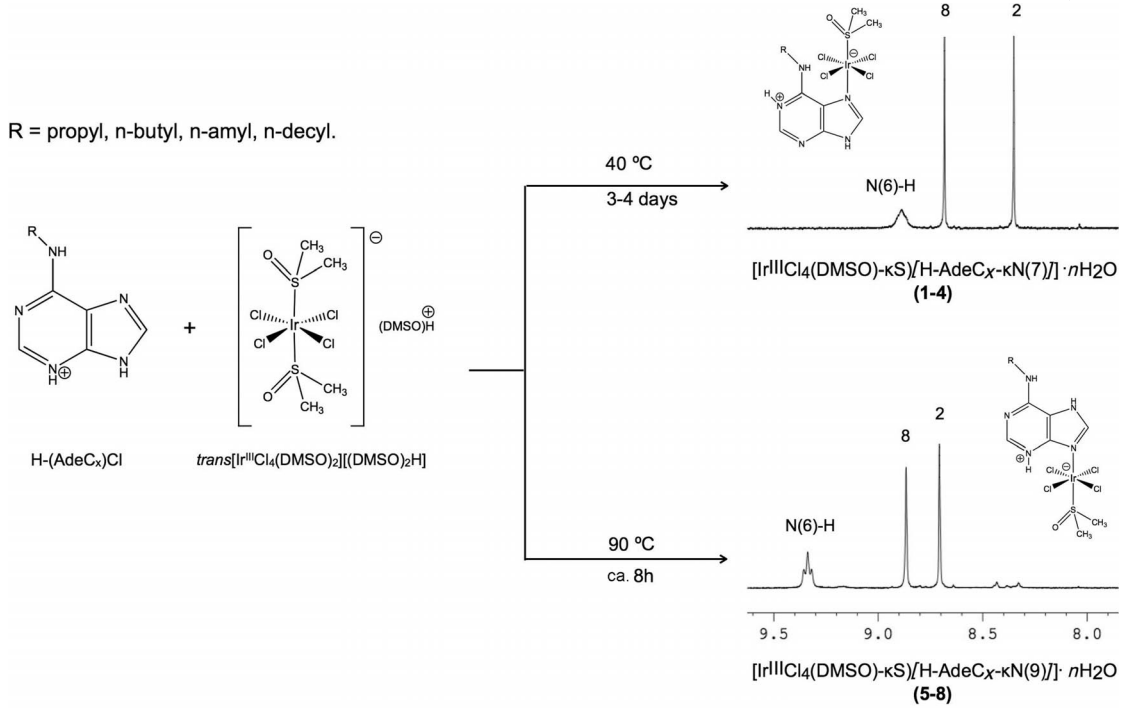

Scheme 2. Synthetic route to **1**–**8**.

Table 2. Selected ^{1}H NMR signals [ppm] for N^6-alkyladenine hydrochlorides and complexes **1**–**8**.

N^6-Propyladenine (L)					
	L·HCl	L(N7–Ir) **1**	Δδ[a]	L(N9–Ir) **5**	Δδ[a]
2-H	8.54 s	8.36 s	–0.18	8.71 s	+0.17
8-H	8.50 s	8.69 s	+0.19	8.87 s	+0.37
N^6-Butyladenine (L)					
	L·HCl	L(N7–Ir) **2a**	Δδ[a]	L(N9–Ir) **6**	Δδ[a]
2-H	8.56 s	8.26 s	–0.30	8.70 s	+0.14
8-H	8.51 s	8.61 s	+0.10	8.87 s	+0.36
N^6-Pentyladenine (L)					
	L·HCl	L(N7–Ir) **3**	Δδ[a]	L(N9–Ir) **7**	Δδ[a]
2-H	8.54 s	8.34 s	–0.20	8.70 s	+0.16
8-H	8.48 s	8.66 s	+0.18	8.85 s	+0.37
N^6-Decyladenine (L)					
	L·HCl	L(N7–Ir) **4**	Δδ[a]	L(N9–Ir) **8**	Δδ[a]
2-H	8.55 s	8.28 s	–0.27	8.69 s	+0.14
8-H	8.49 s	8.76 s	+0.27	8.82 s	+0.33

[a] $\Delta\delta = \delta$ (complex) – δ (adenine hydrochloride).

according to the literature[41,42] and the most characteristic variations in the bands of the complexes are shown in Table 3. All the spectra show the typical ν(S=O) vibration between 1121 and 1080 cm^{-1}, the $\rho_r(CH_3)$ band at 1017–1026 cm^{-1} and the ν(Ir–S) medium intensity band at approximately 440 cm^{-1}.[14] With respect to the adenine moiety, the spectra of the complexes show small shifts on the two bands at approximately 1660 and 1615 cm^{-1} related to δ(NHR) + ν[C(5)–C(6)] + ν[C(6)–NH$_2$] and more important changes in frequency and intensity of the ν(ring) bands between 1500 and 1300 cm^{-1}. As observed in the ruthenium(III) analogues,[23] the 1513–1526 cm^{-1} weak band assignable to ν[C(4)–N(9)] + δ[C(8)–H] disappears in all spectra of N(9)coordinated compounds with the exception of complex **8**. On the contrary, all the N(7)-coordinated and N(1)-protonated complexes show this characteristic weak band. This spectral change represents a useful IR diagnostic to distinguish between N(9)- and N(7)-coordinated adenine complexes. A second feature to discriminate between N(7)- and N(9)-coordinated adenine complexes is the presence, only in N(9)-coordinated compounds, of a very weak characteristic broad band at approximately 3500 cm^{-1} in the ν(OH) (water) region assignable to H-bond sensitive NH modes.[43]

The electronic spectra of all the obtained Ir^{III} compounds in DMSO solution present a similar pattern. Visible absorption spectra of complexes **2a** and **6** in DMSO (10^{-3} M) are reported in Figure 2. The two weak bands appearing at lower energy: 470 nm [ε = 25 M^{-1}cm^{-1} for **2a**]; 473 nm [ε = 20 M^{-1}cm^{-1} for **6**] and approximately 395 nm [ε = 86 M^{-1}cm^{-1} for **2a** and ε = 66 M^{-1}cm^{-1} for **6**] are tentatively assigned to singlet–triplet transitions $^1A_{1g} \rightarrow {}^3T_{1g} + {}^3T_{2g}$, while the stronger band at approximately 343 nm [ε = 86 M^{-1}cm^{-1} for **2a**] at higher energy to the spin-allowed $^1A_{1g} \rightarrow {}^1T_{1g}$ transition.

Table 3. Selected infrared bands [cm^{-1}] for N^6-alkyladenine hydrochlorides and complexes **1**–**8** (ν: stretching, δ: bending, ρ_r: rocking, s: strong, m: medium, w: weak, br: broad, sh: shoulder).

N^6-Alkyladenine (L)		ν(N–H) + ν(OH)	δ(NHR) + ν[C(5)–C(6)] + ν[C(6)–NH_2]	ν(ring): δ(NH)	ν(ring): ν[C(4)–N(9)] + δ[C(8)–H]	ν(S=O)	$\rho_r(CH_3)$	ν(Ir–S)
Propyl	L–HCl	3377 m	1662 vs, 1615 m	1583 m	1520 w			
	L(N7–Ir) **1**	3537 s, 3470 s, sh	1665 vs, 1604 m	1580 m, sh	1520 w	1107 s	1026 s	442 m
	L(N9–Ir) **5**	3462 w, br	1653 vs, 1610 m	1568 m	–	1084 vs	1021 m	442 m
Butyl	L–HCl		1666 vs, 1614 m	1578 sh, m	1519 m			
	L(N7–Ir) **2a**	3521 m	1671 vs, 1604 m	1576 m, sh	1522 w	1114 m	1024 m	441 m
	L(N9–Ir) **6**	3473 w, br	1665 vs, 1618 m	1581 m	–	1121 m	1017 m	442 m
Pentyl	L–HCl	3476 w	1662 vs, 1615 m	1578 m	1518 m			
	L(N7–Ir) **3**	3524 s, 3437m	1673 vs, 1608 s	1574 m	1521 w	1103 s	1024 s	440 m
	L(N9–Ir) **7**	3500 w, br	1666 vs, 1624 m, sh	1581 m	–	1112 m, 1080 m	1022 m	441 m
Decyl	L–HCl	3535 w, 3444w	1661 vs, 1614 m	1582 m	1513 w			
	L(N7–Ir) **4**	3520 m	1673 vs, 1608 m	1576 m	1521 w	1114 s	1021 s	440 m
	L(N9–Ir) **8**	3500 w, br	1659 vs, 1619 m	1574 m	1514 w	1111 m, 1071 m	1023 m	441 m

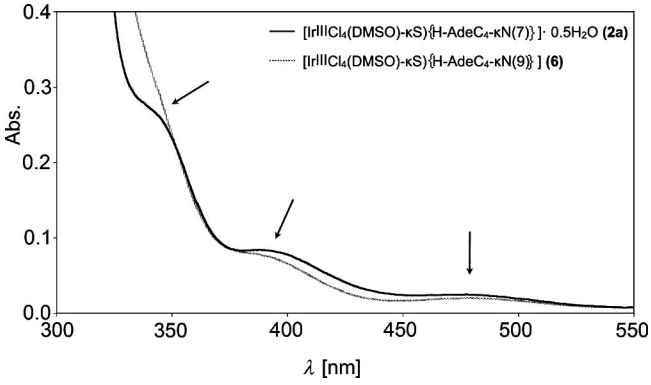

Figure 2. Visible absorption spectra of complexes [$Ir^{III}Cl_4$(DMSO-κS){H-$AdeC_4$-κN(7)}]·0.5H_2O (**2a**) and [$Ir^{III}Cl_4$(DMSO-κS){H-$AdeC_4$-κN(7)}] (**6**) in DMSO (10^{-3} M).

Theoretical Studies

We performed a focussed theoretical study to explain the fact that two isomeric complexes N(7)–Ir and N(9)–Ir can be obtained depending on the experimental conditions (kinetic/thermodynamic). In this theoretical study, we used a model of N^6-alkyladenine in which the alkyl chain was substituted by a methyl group in order to reduce computational costs. In Figure 3 we show the optimized starting, intermediate and final products used in the theoretical mechanistic proposal, which is shown in detail in Figure 4. The relative free energies (kcal/mol in water as solvent) are relative to the lowest energy intermediate, which is **11** for the kinetic route and **14b** for the thermodynamic route. In this figure the kinetic pathway is shown at the top and the thermodynamic one at the bottom. It should be mentioned that transition states have not been computed, as the ligand dissociation involves a progressive increase in the total energy to finally yield the unsaturated complex and the ligand. Conversely, the ligand association involves a progressive stabilization of the system without crossing a transition state, which is similar to what happens in protonation reactions. In addition, we have used the adenine moiety, protonated at N(1) as starting product, because it is the most stable isomer in water. The adenine protonated at N(3) is 1.07 kcal/mol higher in energy than the isomer protonated at N(1) as calculated by the RI-BP86/def2-TZVP level of theory. For the kinetic route, the starting products **9a** and **10**, which are positively and negatively charged, respectively, interact to form a supramolecular complex **11**, which is stabilized through electrostatic and hydrogen-bonding interactions. This complex suffers a ligand dissociation to form the unsaturated complex **12**, which is 15.8 kcal/mol higher in energy than the saturated complex **11**. This intermediate yields the final product **13** [N(7)–Ir isomer] that is 2.9 kcal/mol lower in energy than intermediate **11** and 3.9 kcal/mol lower than the starting products. The thermo-

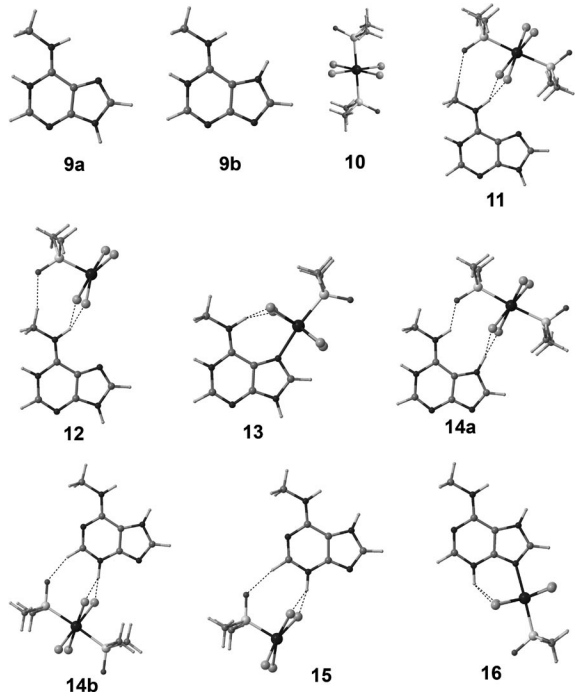

Figure 3. RI-BP86/def2-TZVP optimized structures **9**–**16**.

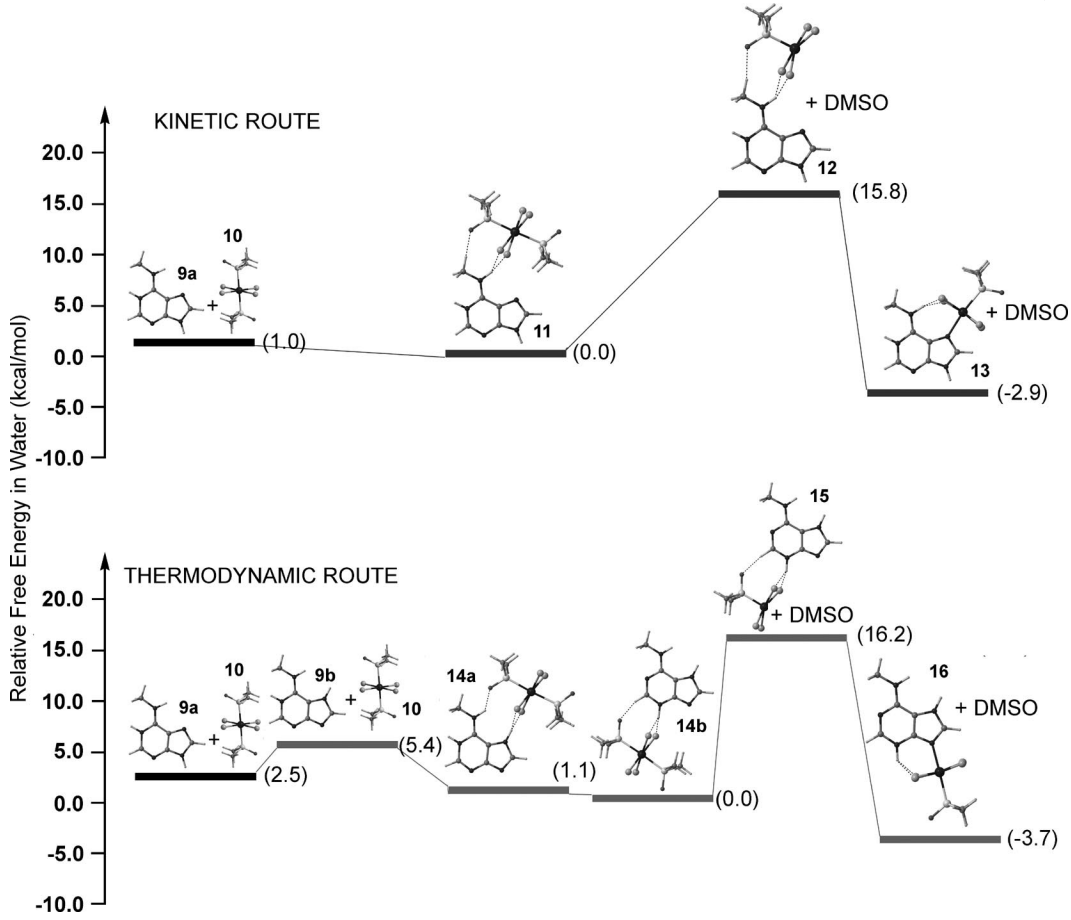

Figure 4. Theoretical mechanistic route to kinetic (top) and thermodynamic (bottom) products. The relative free energies (ΔG [kcal/mol]) are shown in parentheses.

dynamic route (Figure 4, bottom), involves an initial tautomerization of adenine **9a** to adenine **9b**, which is 2.9 kcal/mol higher in energy. This tautomerization is required in order to explain the formation of the final thermodynamic product **16** [N(9)–Ir isomer]. Upon its formation, this tautomeric form **9b** is highly stabilized by electrostatic and hydrogen-bonding interactions by the counterion **10** to form the supramolecular complex **14a** (see Figures 3 and 4). This intermediate is protonated at N1. Since the final product is protonated at N(3), a plausible evolution of this intermediate is the formation of **14b**, where a proton transfer from N(1) to N(3) occurs and a new supramolecular complex forms, in which the iridium complex **10** is located closer to N(9). This intermediate is 1.1 kcal/mol lower in energy than **14a**. This complex undergoes a ligand dissociation to form unsaturated complex **15**, which is 16.2 kcal/mol higher in energy than saturated complex **14b**. The formation of the unsaturated complex from the intermediate is easier by the kinetic (15.8 kcal/mol) than by the thermodynamic (16.2 kcal/mol) pathway. This intermediate yields the final product **16**, which is 3.7 kcal/mol lower in energy than intermediate **14b** and 6.2 kcal/mol lower in energy than the starting products. The N(9)–Ir isomer is lower in energy than the N(7)–Ir isomer, in agreement with the experimental results. This difference in stabilization is probably due to the fact that the charge separation in the zwitterionic final product **13** (similar to complexes **1**–**4**) is large compared that in **16** (similar to complexes **5**–**8**).

Interactions between Iridium Complexes and Plasmid DNA

Atomic force microscopy (AFM) and electrophoretic mobility (Figures 5 and 6, respectively) were used to study the interactions of isolated iridium complexes **1**, **5** and **8** with plasmid pBR322 DNA.

Electrophoretic Mobility, AFM Images and Antiproliferative Activity

The influence of the compounds on the tertiary structure of DNA was determined by its ability to modify the electrophoretic mobility of the covalently closed circular (CCC) and open circular (OC) forms of plasmid pBR322 DNA. In Figure 5, the pattern of electrophoretic mobility of free plasmid pBR322 DNA and plasmid pBR322 DNA incubated with compounds **1**, **5** and **8** is shown in comparison with cisplatin behaviour. Only in the case of compound **8** a slight delay of the CCC form and a decrease in the amount of the OC form were observed. Compounds **1** and **5** do not

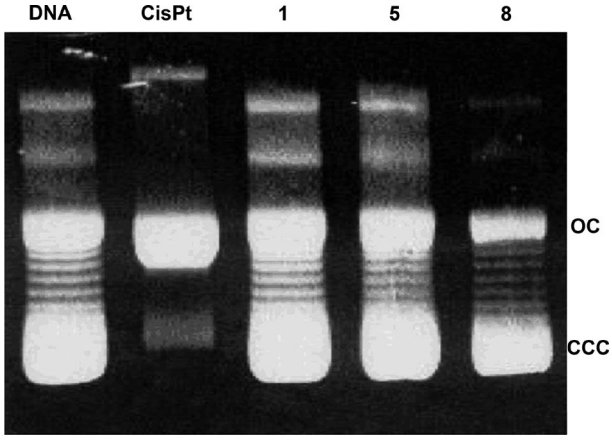

Figure 5. Electrophoresis experiments: plasmid pBR322 DNA (DNA control) incubated in the presence of: *cis*-$Pt(NH_3)_2Cl_2$, [$Ir^{III}Cl_4$(DMSO-κS){H-AdeC$_3$-κN(7)}]·3H_2O (**1**), [$Ir^{III}Cl_4$(DMSO-κS){H-AdeC$_3$-κN(9)}] (**5**) and [$Ir^{III}Cl_4$(DMSO-κS){H-AdeC$_{10}$-κN(9)}] (**8**).

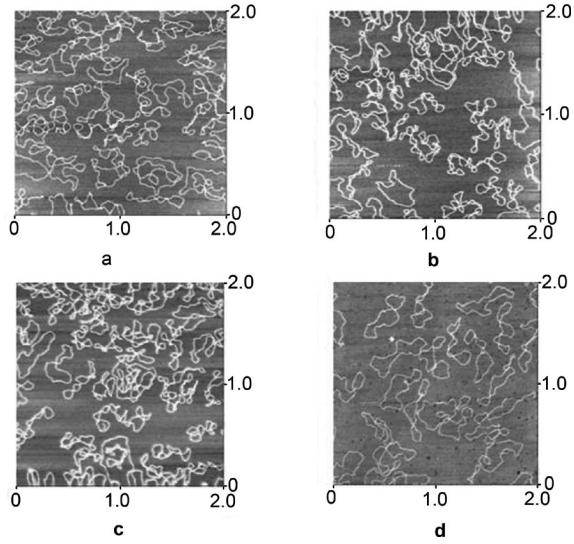

Figure 6. AFM images: plasmid pBR322 DNA incubated 5 h at 37 °C with (a) [$Ir^{III}Cl_4$(DMSO-κS){H-AdeC$_3$-κN(7)}]·3H_2O (**1**), (b) [$Ir^{III}Cl_4$(DMSO-κS){H-AdeC$_3$-κN(9)}] (**5**), (c) [$Ir^{III}Cl_4$(DMSO-κS){H-AdeC$_{10}$-κN(9)}] (**8**) and (d) control.

seem to modify the tertiary structure of the plasmid DNA.

An AFM image of plasmid pBR322 DNA without previous treatment, in mixed covalently closed circular (CCC) and open circular (OC) forms, is shown in Figure 6d. The images obtained of plasmid pBR322 DNA incubated with (a) compound **1**, (b) compound **5**, and (c) compound **8** show the same type of modification of the plasmid forms: the number of supercoiled forms and the grade of supercoiling increases in comparison with free DNA plasmid, (d). These three complexes interact with DNA to modify its structure, mainly producing supercoiling and kinks in the plasmid forms in comparison with free DNA plasmid.

Compounds **1**, **5** and **8** were also assayed against the tumour cell line HL-60. The IC_{50} (μM, 72 h) values obtained against HL-60 cells are very high [>200 μM in **1** and **5** and >150 μM in **8** vs. 2.15± 0.1 in the cisplatin control] in comparison with those obtained for analogous octahedral ruthenium(III) NAMI-A type compounds. Although similar [$Ru^{III}Cl_4$(DMSO)L] complexes with L = purine ligands are only weakly active on tumour TS/A murine adenocarcinoma cell proliferation,[44] the dmtp (dmtp = 5,7-dimethyl)[1,2,4] triazolo[1,5-*a*]pyrimidine derivative inhibits metastasis growth in vivo (MCa mammary carcinoma tumours), being noncytotoxic on tumour TS/A murine adenocarcinoma cells like NAMI-A.[45] In addition, compounds of the 3-pyridinehydroxamic acid and 4-pyridinehydroxamic acid NAMI-A type were devoid of any meaningful cytotoxicity against the cell lines tested. However, the 3-pyridinehydroxamic acid derivative inhibited tumour cell invasion of the highly invasive MDA-MB-231 cells.[16] Such inactivity for the Ir^{III} complexes is related to their inertness and difficulty to be involved in ligand exchange processes. Octahedral iridium(III) complexes that are biologically poorly active are devoid of redox properties and could be useful as tracing systems to study the route of Ru^{III} analogues. Similar results have been obtained with Ir^{III}-imidazole related systems.[11,12,21]

Conclusions

We have synthesized new chlorido(dimethyl sulfoxide)-iridium(III) complexes with N^6-substituted adenine derivatives. We have observed that the substitution in N(7) or in N(9) of the adenine can be controlled experimentally (kinetic or thermodynamic conditions). Both isomers have been characterized by means of X-ray crystallography. A theoretical explanation for the experimental results has been provided by using high-level DFT calculations. We have proposed a mechanistic pathway that agrees with the experimental findings. Finally, preliminary biological assays (AFM images) show interaction between Ir complexes and plasmid pBR322 DNA; however, no antiproliferative properties against the tumour cell line HL-60 have been observed.

Experimental Section

Materials, Analysis and Physical Measurements: All organic and inorganic reagents were purchased from Sigma–Aldrich and used without further purification. Elemental analyses were carried out with Carlo Erba instrument models 1106 and 1108 and Thermo Finnigan Flash 1112 microanalyzers. Infrared spectra were obtained in the solid phase with KBr pellets by using a Bruker IFS 66 instrument. UV/Vis spectra were recorded with a Varian Cary 300 Bio UV/Vis spectrophotometer. ^1H and ^{13}C NMR spectra were recorded with a Bruker AMX 300 spectrometer. Proton and carbon chemical shifts in dimethyl sulfoxide were referenced to [D_6]DMSO itself [^1H NMR (DMSO): δ = 2.47 ppm. ^{13}C NMR (DMSO): δ = 40.0 ppm].

DNA Interaction Studies (Formation of Drug–DNA Complexes): Deionized Milli-Q water (18.2 MW) was filtered through 0.2 nm FP030/3 filters (Schleicher & Schuell) and centrifuged at 4.000 g prior to use. pBR322 DNA was heated at 60 °C for 10 min to ob-

tain the open circular (OC) form. To stock aqueous solutions of plasmid pBR322 DNA in Hepes buffer (4 mM Hepes, pH 7.4/2 mM $MgCl_2$) were added aqueous solutions (with 4% of DMSO) of complexes in a 10:1 ratio of DNA base pair to complex. In parallel experiments, blank samples of free DNA and DNA complex solutions were equilibrated at 37 °C for 4 h in the dark shortly thereafter.

AFM Imaging: Samples were prepared by casting a 3 μL drop of test solution onto freshly cleaved mica disks as support. The drop was kept undisturbed for 3 min to favour the interaction between adsorbate and substrate. Each DNA-laden disk was rinsed with Milli-Q water and was blown dry with clean compressed argon gas directed normal to the disk surface. Samples were stored over silica prior to AFM imaging. All AFM observations were made with a Nanoscope III Multimode AFM instrument (Digital Instrumentals, Santa Barbara, CA). Nanocrystalline Si cantilevers of 125 nm length with a spring constant of 50 N/m average ending with conical-shaped Si probe tips of 10 nm apical radius and 35° cone angle were utilized. High-resolution topographic AFM images were performed in air at room temperature (relative humidity < 40%) on different specimen areas of 2 × 2 μm operating in the intermittent contact mode at a rate of 1–3 Hz.

Agarose Gel Electrophoresis: PBR322 DNA aliquots (0.25 μg/mL) were incubated in TE buffer (10 mM Tris·HCl, 1 mM EDTA, pH = 7.5) at a molar ratio r_i = 0.50 for the electrophoresis study. Incubation was carried out in the dark at 37 °C for 24 h. Charge marker (4 μL) was added to the compound–DNA complex (20 μL). Electrophoresis of the mixture was performed in agarose gel (1% in TBE buffer, Tris-Borate-EDTA) for 5 h at 1.5 V/cm. Afterwards, the DNA was dyed with ethydium bromide solution (0.75 μg/mL in TBE) for 6 h. A sample of free DNA was used as control. The experiment was carried out in an ECOGEN horizontal tank connected to a PHARMACIA GPS 200/400 variable potential power supply, and the gel was photographed with an image Master VDS instrument from Pharmacia Biotech.

Growth Inhibition Assays: Antiproliferative activity of the iridium complexes and cisplatin was tested in a cell culture system with the human acute promyelocytic leukaemia cell line HL-60 [American Type Culture Collection (ATCC)]. The cells were grown in RPMI-1640 medium supplemented with 10% (v/v) heat-inactivated fetal bovine serum and glutamine (2 mmol/L, Life Technologies, Inc.) in a highly humidified atmosphere of 95% air with 5% CO_2 at 37 °C. The growth inhibitory effect was measured by the microculture tetrazolium [3-(4,5-dimethylthiazol-2-yl)-2,5-diphenyltetrazolium bromide, MTT] assay.[46] Following the addition of different concentrations of the complex to quadruplicate wells, plates were incubated at 37 °C for 24 or 72 h. Aliquots (20 mL) of MTT solution were then added to each well. After 3 h, the colour formed was quantitated by a spectrophotometric plate reader (Labsystems iEMS Reader MF) at 490 nm. Cytotoxicity was evaluated in terms of cell growth inhibition in treated cultures relative to that in untreated controls. IC50, the concentration of compound at which cell proliferation was 50% of that observed in control cultures, was obtained by using the GraphPad Prism software, version 4.0.

Synthesis of N^6-Alkyladenines (AdeC$_x$) and Their Hydrochlorides H-(AdeC$_x$)Cl: N^6-alkyladenines (AdeC$_x$) were easily prepared in good yield by a procedure previously described from 6-chloropurine and the corresponding alkylamine under reflux in BuOH/Et_3N.[23,24,47] Dissolution of all these compounds in HCl (2 M) yielded the corresponding hydrochloride salts.

[(DMSO)$_2$H][trans-Ir^{III}Cl$_4$(DMSO)$_2$]: The starting complex, [(DMSO)$_2$H][*trans*-Ir^{III}Cl$_4$(DMSO)$_2$], was prepared according to the procedure published by Haddad et al.[48]

[Ir^{III}Cl$_4$(DMSO-κS){H-AdeC$_x$–κN(7)}]·*n*H$_2$O: The corresponding N^6-alkyladenine hydrochloride [H-AdeC$_x$]Cl (0.19 mmol) was dissolved in distilled water (3 mL) and heated, in an oil bath, at 40 °C. An equimolar quantity of [(DMSO)$_2$H][*trans*-Ir^{III}Cl$_4$(DMSO)$_2$] (123 mg, 0.19 mmol), dissolved in distilled water or methanol (3 mL), was added, and the solution was kept at 40 °C without stirring for 3–4 d (see below). Orange crystals appeared in the solution, which were filtered off, washed with cold water and dried under vacuum. The procedure is shown in Scheme 2.

[Ir^{III}Cl$_4$(DMSO-κS){H-AdeC$_3$-κN(7)}]·3H$_2$O (1): Orange prismatic crystals (160 mg, 25%) suitable for X-ray diffraction crystallography were obtained in water after 3 d. $C_{10}H_{18}Cl_4IrN_5OS·3H_2O$ (644.42): calcd. C 18.64, H 3.75, N 10.87; found C 18.41, H 3.59, N 10.54. IR: ṽ = 3537 (s), 3470 (s), 2385 (m), 1665 (vs), 1604 (s), 1580 (m, sh), 1520 (w), 1459 (m), 1425 (m), 1400 (m), 1340 (m), 1314 (m), 1179 (m), 1107 (s), 1026 (s), 919 (m), 880 (m), 545 (m), 442 (m) cm^{-1}. ^{1}H NMR: δ = ([D$_6$]DMSO): 8.89 [br. s, 1 H, N(6)-H], 8.69 [s, 1 H, 8-H], 8.36 [s, 1 H, 2-H], 1.63 [q, J = 7.2 Hz, 2 H, 11-H], 0.96 [t, J = 7.2 Hz, 3 H, 12-H] ppm. ^{13}C NMR: ([D$_6$]-DMSO): = 149.8 [C-6], 149.5 [C-2], 148.1 [C-4], 148.0 [C-8], 117.2 [C-5], 43.6 [C-10], 22.1 [C-11], 12.2 [C-12] ppm. When the above reaction was carried out at 25 °C, a pale-yellow microcrystalline material appeared immediately, which corresponds to the outer-sphere complex [H-AdeC$_3$][Ir^{III}Cl$_4$(DMSO-κS)$_2$] (160 mg, 24%). $C_{12}H_{24}Cl_4N_5IrO_2S_2$ (668.51): calcd. C 21.56, H 3.62, N 10.48; found C 21.63, H 3.51, N 10.26. IR: ṽ = 3288 (m), 3213 (m), 3160 (w, sh), 3071 (m), 3008 (m), 2988 (m), 1663 (vs), 1610 (m), 1575 (w, sh), 1438 (vs), 1400 (s), 1371 (m), 1341 (m), 1316 (m 1279 (m), 1206 (m), 1155 (s), 1100 (vs), 1017 (s), 777 (m), 618 (s), 538 (w, sh), 530 (m), 427 (m) cm^{-1}. ^{1}H NMR ([D$_6$]DMSO): δ = 8.53 [br. s, 1 H, 2-H], 8.44 [s, 1 H, 8-H], 3.49 [br. s, 2 H, 10-H], 1.63 [sext., J = 7.2 Hz, 2 H, 11-H], 0.91 [t, J = 7.2 Hz, 3 H, 12-H] ppm. After 48 h at 25 °C, orange crystals corresponding to the coordinated compound [Ir^{III}Cl$_4$(DMSO-κS){H-AdeC$_3$-κN(7)}]·3H$_2$O **(1)** were isolated from the mother liquor.

[Ir^{III}Cl$_4$(DMSO-κS){H-AdeC$_4$-κN(7)}]·0.5·H$_2$O (2a): Orange microcrystalline material (233 mg, 38%) was obtained in water after 4 d. $C_{11}H_{20}Cl_4IrN_5OS·0.5H_2O$ (613.41): calcd. C 21.54, H 3.45, N 11.42; found C 21.58, H 3.55, N 11.34. IR: ṽ = 3521 (m), 1671 (vs), 1604 (m), 1576 (m, sh), 1522 (w), 1420 (s), 1209 (m), 1114 (s), 1024 (s), 775 (m), 441 (m) cm^{-1}. ^{1}H NMR: δ = ([D$_6$]DMSO): 8.61 [s, 1 H, 8-H], 8.25 [s, 1 H, 2-H], 1.57 [br. quint., $J_{est.}$ = 7.2 Hz, 2 H, 11-H], 1.42 [br. sext., $J_{est.}$ = 7.2 Hz, 2 H, 12-H], 0.87 [t, J = 7.2 Hz, 3 H, 13-H] ppm. In addition, suitable orange crystals for X-ray diffraction of composition [Ir^{III}Cl$_4$(DMSO-κS){H-AdeC$_4$-κN(7)}]·3H$_2$O **(2b)** were obtained from the mother liquor.

[Ir^{III}Cl$_4$(DMSO-κS){H-AdeC$_5$-κN(7)}] (3): A pale-orange precipitate (68 mg, 11%) was obtained in water after 4 d. $C_{12}H_{22}Cl_4IrN_5OS$ (618.43): calcd. C 23.31, H 3.59, N 11.32; found C 23.78, H 3.87, N 11.47. IR: ṽ = 3524 (s), 3437 (m), 1673 (vs), 1608 (s), 1574 (m), 1521 (w), 1463 (w), 1420 (vs), 1395 (m), 1206 (s), 1137 (vs), 1103 (s), 1024 (s), 982 (m), 916 (m), 809 (m), 553 (m), 440 (m) cm^{-1}. ^{1}H NMR ([D$_6$]DMSO): δ = 8.76 [br. t, 1 H, N(6)-H], 8.66 [s, 1 H, 8-H], 8.34 [s, 1 H, 2-H], 3.45 [br. m, 2 H, 10-H], 1.62 [br. quint., J = 6.9 Hz, 2 H, 11-H], 1.35 [br. m, 4 H, 12-H/13-H], 0.85 [t, J = 6.9 Hz, 3 H, 14-H] ppm.

[Ir^{III}Cl$_4$(DMSO-κS){H-AdeC$_{10}$-κN(7)}]·0.33H$_2$O (4): A pale-orange precipitate (180 mg, 26%) was obtained in methanol after 3 d at 65 °C. $C_{17}H_{32}Cl_4IrN_5OS·0.33H_2O$ (694.51): calcd. C 29.40,

H 4.74, N 10.08; found C 29.42, H 4.53, N 9.81. IR: $\tilde{\nu}$ = 3520 (m), 1673 (vs), 1608 (m), 1576 (m), 1521 (w), 1415 (m), 1114 (s), 1021 (s), 440 (m) cm^{-1}. ^1H NMR ([D$_6$]DMSO): δ = 8.76 [s, 1 H, 8-H], 8.28 [s, 1 H, 2-H], 8.14 [br. s, 1 H, N(6)-H], 4.31 [br. t, 2 H, 10-H], 1.75 [br. m, 2 H, 11-H], 1.21 [br. m, 14 H, 12-H to 18-H], 0.82 [br. t, 3 H, 19-H] ppm.

[Ir^{III}Cl$_4$(DMSO-κS){H-AdeC$_x$–κN(9)}]: The corresponding N^6-alkyladenine hydrochloride [H-AdeC$_x$]Cl (0.19 mmol) was dissolved in distilled water (3 mL) and heated in an oil bath, at 90 °C. [(DMSO)$_2$H][*trans*-Ir^{III}Cl$_4$(DMSO)$_2$] (246 mg, 0.38 mmol), dissolved in distilled water or methanol (3 mL), was added, and the solution was kept at 90 °C without stirring for several hours (see below). Orange microcrystals appeared in the solution, which were filtered off, washed with cold water and dried under vacuum (Scheme 2).

[Ir^{III}Cl$_4$(DMSO-κS){H-AdeC$_3$-κN(9)}] (5): Orange prismatic crystals (236 mg, 40%) suitable for X-ray diffraction crystallography were obtained in water after 8 h. $C_{10}H_{18}Cl_4IrN_5OS$ (590.38): calcd. C 20.34, H 3.07, N 11.86; found C 20.39, H 3.07, N 11.67. IR: $\tilde{\nu}$ = 3462 (w, br), 1653 (vs), 1610 (m), 1568 (m), 1456 (m), 1402 (m), 1356 (m), 1084 (vs), 1021 (m), 442 (m) cm^{-1}. ^1H NMR: δ = ([D$_6$]-DMSO): 9.34 [br. t, 1 H, N(6)-H], 8.87 [s, 1 H, 8-H], 8.71 [s, 1 H, 2-H], 3.62 [br. m, 2 H, 10-H], 1.65 [sext., J = 7.2 Hz, 2 H, 11-H], 0.93 [t, J = 7.2 Hz, 3 H, 12-H] ppm. ^{13}C NMR ([D$_6$]DMSO): δ = 153.1 [C-6], 148.6 [C-8], 146.9 [C-2], 145.0 [C-4], 112.4 [C-5], 43.4 [C-10], 22.2 [C-11], 11.8 [C-12] ppm.

[Ir^{III}Cl$_4$(DMSO-κS){H-AdeC$_4$-κN(9)}] (6): Orange microcrystals (447 mg, 74%) were obtained in water after 8 h. $C_{11}H_{20}Cl_4IrN_5OS$ (604.40): calcd. C 21.86, H 3.34, N 11.59; found C 22.03, H 3.27, N 11.52. IR: $\tilde{\nu}$ = 3473 (w, br), 1665 (vs), 1618 (m), 1581 (m), 1449 (m), 1410 (w), 1378 (w), 1121 (m), 1017 (m), 609 (w), 563 (w), 442 (m) cm^{-1}. ^1H NMR ([D$_6$]DMSO): δ = 9.30 [br. s, 1 H, N(6)-H], 8.85 [s, 1 H, 8-H], 8.70 [s, 1 H, 2-H], 1.61 [quint., J = 7.5 Hz, 2 H, 11-H], 1.36 [sext., J = 7.5 Hz, 2 H, 12-H], 0.89 [t, J = 7.5 Hz, 3 H, 13-H] ppm. ^{13}C NMR ([D$_6$]DMSO): δ = 153.0 [C-6], 148.5 [C-8], 147.0 [C-2], 145.0 [C-4], 112.3 [C-5], 41.4 [C-10], 30.9 [C-11], 20.0 [C-12], 14.1 [C-13] ppm.

[Ir^{III}Cl$_4$(DMSO-κS){H-AdeC$_5$-κN(9)}] (7): An orange precipitate (310 mg, 50%) was obtained in water after 8 h. $C_{12}H_{22}Cl_4IrN_5OS$ (618.43): calcd. C 23.31, H 3.59, N 11.32; found C 23.33, H 3.49, N 11.36. IR: $\tilde{\nu}$ = 3500 (br, w), 1666 (vs), 1624 (m, sh), 1581 (m), 1474 (m, sh), 1444 (m), 1406 (m), 1378 (m), 1112 (m), 1080 (m), 1022 (m), 774 (m), 665 (m), 441 (m) cm^{-1}. ^1H NMR ([D$_6$]DMSO): δ = 9.31 [br. s, 1 H, N(6)-H], 8.85 [s, 1 H, 8-H], 8.70 [s, 1 H, 2-H], 3.63 [br. t, 2 H, 10-H], 1.62 [br. t, 2 H, 11-H], 1.31 [br. s, 4 H, 12-H/13-H], 0.86 [br. t, 3 H, 14-H] ppm. ^{13}C NMR ([D$_6$]DMSO): δ = 153.1 [C-6], 148.7 [C-8], 146.8 [C-2], 145.1 [C-4], 112.8 [C-5], 41.7 [C-10], 28.9 [C-11], 28.6 [C-12], 22.3 [C-13], 14.4 [C-14] ppm.

[Ir^{III}Cl$_4$(DMSO-κS){H-AdeC$_{10}$-κN(9)}] (8): Orange microcrystals (537 mg, 78%) were obtained in methanol after 4 days. $C_{17}H_{32}Cl_4IrN_5OS$ (688.56): calcd. C 29.65, H 4.68, N 10.17; found C 29.53, H 4.52, N 9.94. IR: $\tilde{\nu}$ = 3500 (w, br), 1659 (vs), 1619 (m), 1574 (m), 1514 (w), 1438 (m), 1400 (m), 1111 (m), 1071 (m), 1023 (m), 790 (w, br), 611 (m), 441 (m) cm^{-1}. ^1H NMR ([D$_6$]DMSO): δ = 9.29 [br. s, 1 H, N(6)-H], 8.82 [s, 1 H, 8-H], 8.69 [s, 1 H, 2-H], 3.62 [br. q, 2 H, 10-H], 1.61 [br. t, 2 H, 11-H], 1.20 [br. m, 14 H, 12-H to 18-H], 0.81 [br. t, 3 H, 19-H] ppm. ^{13}C NMR ([D$_6$]DMSO): δ = 152.8 [C-6], 148.3 [C-8], 147.0 [C-2], 144.8 [C-4], 111.9 [C-5], 41.6 [C-10], 31.7, 29.4, 29.1, 28.8, 26.7, 22.5 [C-11, C-12, C-13, C-14, C-15, C-16, C-17, C-18], 14.4 [C-19] ppm.

Crystallographic Studies: Suitable crystals of **1**, **2b** and **5** were selected for single-crystal X-ray diffraction experiments and mounted at the tip of glass fibres on an Enraf–Nonius CAD4 diffractometer producing graphite monochromated Mo-K_α radiation (λ =

Table 4. Selected crystallographic data for the compounds **1**, **2b** and **5**.

	1	**2b**	**5**
Empirical formula	$C_{10}H_{24}Cl_4IrN_5O_4S$	$C_{11}H_{26}Cl_4IrN_5O_4S$	$C_{10}H_{18}Cl_4IrN_5OS$
MW	644.43	658.43	589.38
Wavelength [Å]	0.71073	0.71073	0.71073
Crystal system	monoclinic	monoclinic	monoclinic
Space group	*P*121/*c*1	*P*21/*n*	*P*21/*c*
a [Å]	8.331(3)	8.375(5)	8.172(2)
b [Å]	27.169(6)	27.340(16)	13.046(2)
c [Å]	12.416(3)	9.316(2)	18.960(2)
β [°]	131.34(2)	90.23(4)	115.53(2)
V [Å^3]	2110.0(12)	2133.1(18)	1824.0(6)
Z	4	4	4
D_{calc} [Mg/m^3]	2.028	2.050	2.142
Absorption coefficient [mm^{-1}]	6.958	6.885	8.026
Crystal size [mm]	0.36 × 0.28 × 0.21	0.49 × 0.41 × 0.3	0.21 × 0.12 × 0.12
θ range for data coll. [°]	1.50–24.98	1.49–25.97	1.96–24.96
Index ranges	$-9 \le h \le 7$	$10 \le h \le 10$	$-9 \le h \le 8$
	$0 \le k \le 32$	$0 \le k \le 33$	$0 \le k \le 15$
	$0 \le l \le 14$	$0 \le l \le 11$	$0 \le l \le 22$
Reflections collected	3696	4444	3570
Independent reflections	3696	4185 [*R*(int) = 0.0446]	3210 [*R*(int) = 0.0472]
Max. and min. transmission	0.232 and 0.116	0.044 and 0.127	0.38 and 0.21
Data/restraints/parameters	3696/354/307	4185/23/237	3210/0/202
Final *R* indices [$I > 2\sigma(I)$]	R_1 = 0.0481	R_1 = 0.0509	R_1 = 0.0412
	wR_2 = 0.1222	wR_2 = 0.1215	wR_2 = 0.0931
R indices (all data)	R_1 = 0.0697	R_1 = 0.0917	R_1 = 0.0671
	wR_2 = 0.1347	wR_2 = 0.1509	wR_2 = 0.1001
GOF on F^2	1.046	1.235	1.027
Largest diff. peak/hole [e Å^{-3}]	1.447/–1.889	3.726/–3.948	1.115/–1.323

0.71073 Å). In each case, after the random search of 25 reflections, the indexation procedure gave rise to the cell parameters (see Table 4 for a summary of the crystal data). Intensity data were collected in the ω-2θ scan mode and corrected for Lorenz and polarization effects. The absorption correction for the three crystals was performed by following the empirical DIFABS method.[49] The structural resolution procedure was carried out with the WinGX package.[50] Solving for structure factor phases was performed with SIR2004[51] for **1** and **2b** and SHELXS-86[52] for **5**, and full-matrix refinement was done with SHELXL97.[53] Non-H atoms were refined anisotropically and H atoms were introduced in calculated positions and refined as riding on their parent atoms, except for water molecules and the protonation site in **1**, where H atoms were located in difference Fourier maps and refined isotropically. Hydrogen atoms belonging to water molecules in **2b** could not be located in difference Fourier maps. In **1**, the aliphatic chain presents rotational disorder, which has been modelled by assuming three fragments with complementary occupancies (50%, 25% and 25% respectively). Due to the disorder model applied in **1**, ISOR and DELU instructions have been used to make the ellipsoids much more realistic, consequently a large number of restraints are generated (see Table 4), which also lists a summary of refinement parameters. Selected bond lengths and angles around the metal ion are shown in Table 1.

Computational Details: The geometries of all complexes studied in this work were fully optimized at the RI-BP86/def2-TZVP level of theory by using the program TURBOMOLE version 5.7.[54] The def2-TZVP is a Gaussian atomic orbital (AO) basis set of triple-ζ quality augmented with polarization functions.[55] This basis set uses relativistic effective core potential (ECP) for the iridium atom. For some supramolecular complexes, the C_s symmetry constraint has been imposed. The RI-DFT method applied to the study of weak interactions is considerably faster than the DFT method, and the interaction energies and equilibrium distances are almost identical for both methods.[56] We have performed the calculations in the presence of solvent (water, dielectric constant ε = 78.39) by using the conductor-like screening model (COSMO)[57] as implemented in TURBOMOLE.

CCDC-771877 for **1**, -771878 for **2b** and -771879 for **5** contain the supplementary crystallographic data for this paper. These data can be obtained free of charge from The Cambridge Crystallographic Data Centre via www.ccdc.cam.ac.uk/data_request/cif.

Acknowledgments

We thank the Dirección General de Investigación Ciencia y Tecnología [DGICYT] of Spain (projects CTQ2008-00841/BQU and CTQ2006-09339/BQU) and the Direcció General de Recerca, Desenvolupament Tecnològic i Innovació del Govern Balear for financial support. We thank the Centre de Supercomputació de Catalunya [CESCA] for computational facilities. F. M. A. thanks the Conselleria d'Economia, Hisenda i Innovació del Govern de les Illes Balears (Spain) and Fons Social Europeu [FSE] for a contract as "investigation support technician". Y. L. acknowledges a fellowship from Fundación Carolina (MAE, Spain). C. E. thanks the Ministerio de Educación y Ciencia [MEC] of Spain for a predoctoral fellowship. D. Q. thanks the Ministerio de Ciencia e Innovación [MICINN] of Spain for a "Ramón y Cajal" contract. The authors wish to thank Prof. Francesc X. Avilés and Dr. Julia Lorenzo for performing the cytotoxic assays for all the tested compounds. Financial support from the Ministerio de Ciencia e Innovación [MICINN] of Spain (CTQ2009-12520-C03-03) and Consolider Ingenio 2010 (CSD2007-00041) and DURSI-Generalitat de Catalunya (2009SGR-203) are gratefully acknowledged. I. M. thanks the Institut de Ciència de Materials de Barcelona [ICMAB] for a JAEDoc fellowship financed by the European Social Fund.

[1] L. A. Oro, C. Claver (Eds.), *Iridium Complexes in Organic Synthesis*, Wiley-VCH, Weinheim, **2009**.
[2] A. B. Tamayo, G. Simona, T. Sajoto, P. I. Djurovich, I. M. Tsyba, R. Bau, M. E. Thompson, *Inorg. Chem.* **2005**, *44*, 8723–8732.
[3] S. Lamansky, P. Djurovich, D. Murphy, F. Abdel-Razzaq, H. Lee, C. Adachi, P. E. Burrows, S. R. Forrest, M. E. Thompson, *J. Am. Chem. Soc.* **2001**, *123*, 4304–4312.
[4] F. Shao, B. Elias, W. Lu, J. K. Barton, *Inorg. Chem.* **2007**, *46*, 10187–10199.
[5] K. K. Lo, D. C. Ng, C. Chung, *Organometallics* **2001**, *20*, 4999–5001.
[6] K. K. Lo, C. Chung, T. K. Lee, L. Lui, K. H. Tsang, N. Zhu, *Inorg. Chem.* **2003**, *42*, 6886–6897.
[7] D. Herebian, W. S. Sheldrick, *J. Chem. Soc., Dalton Trans.* **2002**, 966–974.
[8] J. M. O'Connor, K. Hiibner, A. L. Rheingold, L. M. Liable-Sands, *Polyhedron* **1997**, *16*, 2029–2035.
[9] K. Yamanari, R. Ito, S. Yamamoto, T. Konno, A. Fuyuhiro, M. Kobayashi, R. Arakawa, *Dalton Trans.* **2003**, 380–386.
[10] C. P. Roy, L. A. Huff, N. A. Barker, M. A. G. Berg, J. S. Merola, *J. Org. Chem.* **2006**, *691*, 2270–2276.
[11] L. Messori, G. Marcon, P. Orioli, M. Fontani, P. Zanallo, A. Bergamo, G. Sava, P. Mura, *J. Inorg. Biochem.* **2003**, *95*, 37–46.
[12] P. Mura, A. Casini, G. Marcon, L. Messori, *Inorg. Chim. Acta* **2001**, *312*, 74–80.
[13] S. Ahrens, T. Strassner, *Acta Crystallogr., Sect. E* **2007**, *63*, 100.
[14] F. M. Albertí, J. J. Fiol, A. García-Raso, M. Torres, A. Terrón, M. Barceló-Oliver, M. J. Prieto, V. Moreno, E. Molins, *Polyhedron* **2010**, *29*, 34–41.
[15] V. Gayathri, E. G. Leelamani, N. M. N. Gowda, G. K. N. Reddy, *Polyhedron* **1997**, *16*, 1169–1176.
[16] D. Griffith, S. Cecco, E. Zangrando, A. Bergamo, G. Sava, C. J. Marmion, *J. Biol. Inorg. Chem.* **2008**, *13*, 511–520.
[17] E. Alessio, *Chem. Rev.* **2004**, *104*, 4203–4242 and references cited therein.
[18] E. Reisner, V. B. Arion, M. F. C. Guedes da Silva, R. Lichtenecker, A. Eichinger, B. K. Keppler, V. Y. Kukushkin, A. J. Pombeiro, *Inorg. Chem.* **2004**, *43*, 7083–7093.
[19] M. A. Scharwitz, I. Ott, R. Gust, A. Kromm, W. S. Sheldrick, *J. Inorg. Biochem.* **2008**, *102*, 1623–1630.
[20] M. Dobroschke, Y. Geldmacher, I. Ott, M. Harlos, L. Kater, L. Wagner, R. Gust, W. S. Sheldrick, A. Prokop, *ChemMedChem* **2009**, *4*, 177–187.
[21] G. Mestroni, E. Alessio, A. S. Santi, S. Geremia, A. Bergamo, G. Sava, A. Boccarelli, A. Schettino, M. Coluccia, *Inorg. Chim. Acta* **1998**, *273*, 62–71.
[22] A. García-Raso, J. J. Fiol, A. Tasada, M. J. Prieto, V. Moreno, I. Mata, E. Molins, T. Bunic, A. Golobic, I. Turel, *Inorg. Chem. Commun.* **2005**, *8*, 800–804.
[23] J. J. Fiol, A. García-Raso, F. M. Albertí, A. Tasada, M. Barceló-Oliver, A. Terrón, M. J. Prieto, V. Moreno, E. Molins, *Polyhedron* **2008**, *27*, 2851–2858.
[24] A. García-Raso, C. Cabot, J. J. Fiol, L. Spichal, J. Nisler, A. Tasada, J. M. Luna, F. M. Albertí, I. V. Sibole, *J. Plant Physiol.* **2009**, *14*, 1529–1536.
[25] D. W. Mok, M. C. Mok, *Annu. Rev. Plant Physiol. Plant Mol. Biol.* **2001**, *89*, 89–118.
[26] K. Dolezal, I. Popa, V. Krystof, L. Spichal, M. Fojtikova, J. Holub, R. Lenobel, T. Schmulling, M. Strnad, *Bioorg. Med. Chem.* **2006**, *14*, 875–884.
[27] L. Meijer, E. Raymond, *Acc. Chem. Res.* **2003**, *36*, 417–425.

[28] P. Starha, Z. Travnicek, R. Herchel, I. Popa, P. Suchy, J. Vanco, *J. Inorg. Biochem.* **2009**, *103*, 432–440 and references cited therein.
[29] Z. Travnicek, I. Popa, M. Cajan, R. Herchel, J. Marek, *Polyhedron* **2007**, *26*, 5271–5282 and references cited therein.
[30] D. J. Hodgson in *Prog. Inorg. Chem. Volume 23* (Ed.: S. J. Lippard), John Wiley and Sons, New York, **1977**, pp. 211–254 and references therein.
[31] M. R. Taylor, *Acta Crystallogr., Sect. B* **1973**, *29*, 884–890.
[32] B. Lippert, D. Gupta, *Dalton Trans.* **2009**, 4619–4634.
[33] P. De Meester, A. C. Skapski, *J. Chem. Soc., Dalton Trans.* **1973**, 424–427.
[34] D. B. Brown, J. W. Hall, H. M. Helis, E. G. Walton, D. J. Hodgson, W. E. Hatfield, *Inorg. Chem.* **1977**, *16*, 2675–2680.
[35] T. Suzuki, Y. Hirai, H. Monjushiro, S. Kaizaki, *Inorg. Chem.* **2004**, *43*, 6435–6444.
[36] Z. Travnicek, M. Malon, Z. Sindelar, K. Dolezal, J. Rolcik, V. Krystof, M. Strnad, J. Marek, *J. Inorg. Biochem.* **2001**, *84*, 23–32.
[37] T. P. Balasubramanian, P. T. Muthiah, Ananthasaravanan, S. K. Mazumdar, *J. Inorg. Biochem.* **1996**, *63*, 175–181.
[38] R. Taylor, O. Kennard, *J. Mol. Struct.* **1982**, *78*, 1.
[39] D. Voet, A. Rich, *Prog. Nucleic Acid Res. Mol. Biol.* **1970**, *10*, 183–265.
[40] L. Messori, G. Marcon, P. Orioli, M. Fontani, P. Zanello, A. Bergamo, G. Sava, P. Mura, *J. Inorg. Biochem.* **2003**, *95*, 37–46.
[41] M. Tsuboi, S. Takahashi, I. Harada in *Physiochemical Properties of Nucleic Acids* (Ed.: J. Duchesne) Academic Press, London, **1973**, vol. 2, pp. 91–145.
[42] M. Tsuboi in *Basic Principles in Nucleic Acid Chemistry* (Ed.: P. O. P. Ts'O) Academic Press, New York, **1974**,vol. 1, pp. 406–416.
[43] A. Dkhissi, L. Houben, L. Adamowicz, G. Maes, *Chem. Phys. Lett.* **2004**, *387*, 362–366.
[44] I. Turel, M. Pecanac, A. Golobic, E. Alessio, B. Serli, A. Bergamo, G. Sava, *J. Inorg. Biochem.* **2004**, *98*, 393–401.
[45] A. H. Velters, A. Bergamo, E. Alessio, E. Zangrando, J. G. Haasnoot, C. Casarsa, M. Cocchietto, S. Zorzet, G. Sava, *J. Med. Chem.* **2004**, *47*, 1110–1121.
[46] I. Vermes, C. Haanen, H. Steffens-Nakken, C. Reutelingsperger, *J. Immunol. Methods* **1995**, *184*, 39–51.
[47] M. Sutherland, B. E. Christensen, *J. Am. Chem. Soc.* **1957**, *79*, 2251–2252.
[48] Y. M. Y. Haddad, H. B. Hembest, J. Troca-Grimshaw, *J. Chem. Soc. Perkin Trans. 1* **1974**, 592–595.
[49] N. Walker, D. Stuart, *Acta Crystallogr., Sect. A* **1983**, *39*, 148–158.
[50] L. J. Farrugia, *J. Appl. Crystallogr.* **1999**, *32*, 837–838.
[51] M. C. Burla, R. Caliandro, M. Camalli, B. Carrozzini, G. L. Cascarano, L. de Caro, C. Giacovazzo, G. Polidori, R. Spagna, *J. Appl. Crystallogr.* **2005**, *38*, 381–388.
[52] G. M. Sheldrick, *SHELXS86*, *Program for the Solution of Crystal Structures*, University of Göttingen, Göttingen, Germany, **1986**.
[53] G. M. Sheldrick, *Acta Crystallogr., Sect. A* **2008**, *64*, 112–122.
[54] R. Ahlrichs, M. Bär, M. Häser, H. Horn, C. Kölmel, *Chem. Phys. Lett.* **1989**, *162*, 165–169.
[55] A. Schäfer, C. Huber, R. Ahlrichs, *J. Chem. Phys.* **1994**, *100*, 5829–5835.
[56] D. Quiñonero, C. Garau, A. Frontera, P. Ballester, A. Costa, P. M. Deyà, *J. Phys. Chem. A* **2006**, *110*, 5144–5157.
[57] A. Klamt, G. Schüürmann, *J. Chem. Soc. Perkin Trans. 2* **1993**, 799–805.

Received: July 29, 2010
Published Online: November 12, 2010

